small
www.small-journal.com

Defect Engineering in Few-Layer Phosphorene

Ankur Sharma, Bo Wen, Boqing Liu, Ye Win Myint, Han Zhang, and Yuerui Lu**

Defect engineering in 2D phosphorene samples is becoming an important and powerful technique to alter their properties, enabling new optoelectronic applications, particularly at the infrared wavelength region. Defect engineering in a few-layer phosphorene sample via introduction of substrate trapping centers is realized. In a three-layer (3L) phosphorene sample, a strong photoluminescence (PL) emission peak from localized excitons at ≈1430 nm is observed, a much lower energy level than free excitonic emissions. An activation energy of ≈77 meV for the localized excitons is determined in temperature-dependent PL measurements. The relatively high activation energy supports the strong stability of the localized excitons even at elevated temperature. The quantum efficiency of localized exciton emission in 3L phosphorene is measured to be approximately three times higher than that of free excitons. These results could enable exciting applications in infrared optoelectronics.

1. Introduction

Phosphorene has been demonstrated as a viable option for the 2D material-based devices and optoelectronic applications because of its universal direct bandgap nature and wide-ranging bandgaps from 0.3 eV (bulk) to 1.7 eV (monolayer).[1–8] Phosphorene serves as a perfect alternative material to bridge the gap between zero-bandgap graphene and large-bandgap transition metal dichalcogenide (TMD)[9,10] semiconductors for suitable applications in the infrared wavelength range. Owing to its puckered lattice configuration,[11,12] phosphorene possesses quasi-1D excitons and trions with highly enhanced binding energies,[13,14] which is in contrast to other TMD 2D semiconductors[15–18] and will enable several promising novel optoelectronic and excitonic devices. Defect engineering has been demonstrated to be an important technique to modulate the properties of semiconductors for various applications.[19,20] Particularly, defect engineering in 2D materials is critical and promising for the development of novel optoelectronic devices.[21–23] Recently, single-photon emitters have been reported from the defect states in atomically thin TMDs and h-BN.[24,25] Extrinsic defects have also been inducted into TMD materials for enhanced photoluminescence (PL) emission and doping sensitive modulation of the emissions.[26,27] However, defect engineered emissions from TMDs have been reported in visible range with energies >1 eV.[28] In contrast, phosphorene, with relatively lower bandgaps, is a perfect candidate to hold defect emissions in infrared wavelength ranges. Particularly, defect emission at the telecommunication band ≈1550 nm is critical for future chip-based quantum communication technologies.[29] Recently, we successfully realized the defect engineering and triggered the defect emissions at ≈920 nm from monolayer phosphorene samples.[30,31] The emission peak energy in phosphorene shows a red shift with increase of layer number; therefore, defect engineering in few-layered phosphorene samples could further push localized exciton emissions to infrared range, which can enable exciting applications, such as chip-based optical telecommunication.[1,3–5,8,13,32–34]

In this work, we explored the defect engineering in few-layer phosphorene samples, by incorporating extrinsic defects using plasma-enhanced chemical vapor deposition (PECVD) grown oxide substrate. We observed a strong PL peak at ≈1430 nm, from localized excitons in three-layer (3L) phosphorene samples. Incident power dependent PL measurements were performed to confirm the emission nature of localized excitons, which shows a sublinear growth with increasing excitation power. Temperature-dependent PL measurements were also carried out to explore the thermal stability and activation energy (E_a) of the localized excitons with increasing temperatures. E_a in 3L phosphorene was measured to be ≈77 meV, which is a large value indicating relative stability of localized excitons even at higher temperatures (≈263 K). This is in sharp contrast to defect states in TMDs, where defect emissions are only visible at cryogenic temperatures.[28] The overall quantum efficiency of localized exciton emission in 3L phosphorene was measured to approximately three times higher than that of free exciton peak.

A. Sharma, Dr. B. Wen, B. Liu, Y. W. Myint, Prof. Y. Lu
Research School of Engineering
College of Engineering and Computer Science
the Australian National University
Canberra, ACT 2601, Australia
E-mail: yuerui.lu@anu.edu.au
Dr. B. Wen, Prof. H. Zhang
SZU-NUS Collaborative Innovation Center for Optoelectronic Science and Technology
Key Laboratory of Optoelectronic Devices and Systems of Ministry of Education and Guangdong Province
College of Optoelectronic Engineering
Shenzhen University
Shenzhen 518060, P. R. China
E-mail: hzhang@szu.edu.cn
The ORCID identification number(s) for the author(s) of this article can be found under https://doi.org/10.1002/smll.201704556.

DOI: 10.1002/smll.201704556

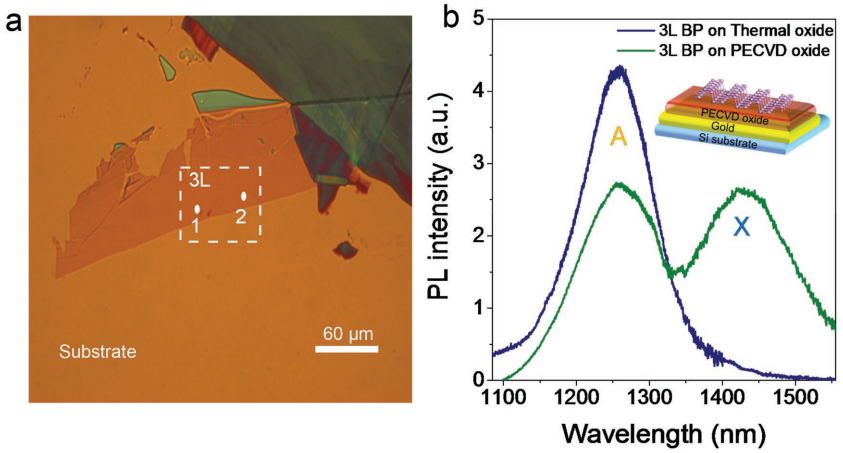

Figure 1. Characterization of 3L phosphorene samples. a) Optical microscope image of the sample used for measurements deposited over PECVD grown oxide layer underneath gold. The dotted square shows the area scanned by PSI to determine the thickness of the sample, hence the layer number (Figure S1b–d, Supporting Information). b) Measured PL spectra from 3L phosphorene at room temperature deposited over thermally grown oxide (blue) and 3L phosphorene sample deposited over PECVD grown oxide (green). Designated free (A) and localized (X) exciton peaks have been marked. Inset shows the schematic diagram of the sample.

2. Results and Discussion

Phosphorene flakes were mechanically exfoliated on to the thermal oxide and PECVD oxide/gold substrates, respectively, under dry conditions. The layer number was first determined by the optical contrast of the layer deposited over the substrate (**Figure 1**a). The sample was then immediately analyzed by a phase-shifting interferometer (PSI) to precisely determine the layer number[35] (Figure S1 and associated text, Supporting Information). PL emission from the two samples on thermal oxide (blue) and PECVD oxide (green) was then measured as shown in the Figure 1b. During the PL measurements, the phosphorene sample was kept at −10 °C in a Linkam microscope-compatible low-temperature chamber, with a continuous flow of liquid nitrogen to sustain the low temperature. At the temperature of −10 °C, the moisture tends to freeze and the photooxidation of phosphorene slows down, which enhances the lifetime of the sample considerably and prevents degradation.[35,36] Also, the sample on PECVD oxide substrate was observed to sustain longer than 24 h as compared to the one on thermal oxide which we observed started to degrade in a few hours. PECVD oxide has a more hydrophobic nature as compared to thermal oxide, which slows down the degradation of phosphorene.[37] According to Andres et al.[38] the degradation rate of phosphorene decreases with increasing thickness. 1L sample can survive up to 30 min in ambient conditions but a 2L, 3L, and 4L sample can survive up to much longer durations. As the layer number increases, the phosphorene samples become mechanically stronger and more stable and can thus survive much higher excitation power. This allowed us to measure PL spectrum at higher excitation power detailed in the following section.[38]

The 3L phosphorene sample on thermal oxide showed a PL peak at ≈1250 nm (designated as A peak, Figure 1b), which is consistent with our previous reports.[14,30,33] In contrast, the 3L phosphorene sample showed two clearly distinctive peaks at 1250 and 1430 nm, assigned as A and X peak, respectively. The peak at 1250 nm was again attributed to the free excitons as it repeats itself from the first case, hence designated as A peak. The peak at 1430 nm (assigned as X peak) is a new feature caused by new PECVD oxide substrate. Also, the PL emission from A peak is reduced as compared to the PL intensity from thermal oxide. We moved the laser excitation spot over the same sample in at least 15 different closely spaced points using a manual piezo-stage controller. The "X" peak is repeatable in all the measurements. However, different PL intensity was observed for "X" peak from different locations, suggesting a nonuniform distribution of defect states, which has been discussed in the later sections.

In order to further study the nature of this new X peak observed, we performed excitation power dependent PL measurements at 263 K. **Figure 2**a shows the various spectrum obtained at various excitation power of the exciting laser from 20 to 110 μW. The PL spectra were fitted by Lorentzian function using two peaks: orange (A peak) and blue (X peak). For further quantitative analysis, the integrated PL intensities of both the peaks were plotted with respect to each other on a log–log scale (Figure 2b). This technique has been described in several previous reports by Yu and co-workers[39] and Heinz and co-workers[40] to determine the nature of excitonic emissions. By fitting the data with a power-law $I_X \propto I_A^{\alpha}$, where I_X is the integrated PL intensity of X peak and I_A is the integrated PL intensity of A peak, it is found that peak X grows sublinearly with the excitation power ($\alpha \approx 0.62$). The sublinear rise in the PL intensity for the 'X' peak was confirmed to be not arising from laser-induced damage of the sample. The PL intensity was repeatable after two cycles of power increase and decrease, suggesting no major damage of the sample. Based on the measured α value, peak X is attributed to the emission of localized excitons. Figure 2c shows the variation of peak energies of both the peaks with increasing laser power. The free exciton peak (peak A) shows a slight blue-shift with increasing laser power. This can be explained by an increase in the quasi-fermi energy level of the exciton pairs due to injection of extra charge carriers at higher excitation power, similar to the phenomenon observed in other 2D quantum well structures.[41] In contrast, the defect peak (peak X) energy does not change with increasing power. The defect energy level in the energy bandgap remains independent of the injection power, possibly due to much lower density of states as compared to the free exciton state.[42] The absolute integrated PL values are plotted as a function of laser power in Figure 2d. The FWHM (Figure 2e) of the A peak increases with the increasing excitation power, which could be attributed to thermal phonon scattering causing the broadening of the PL peak for the free excitons.[43] The X peak is repeatable, as we measured several samples of 3L phosphorene on PECVD

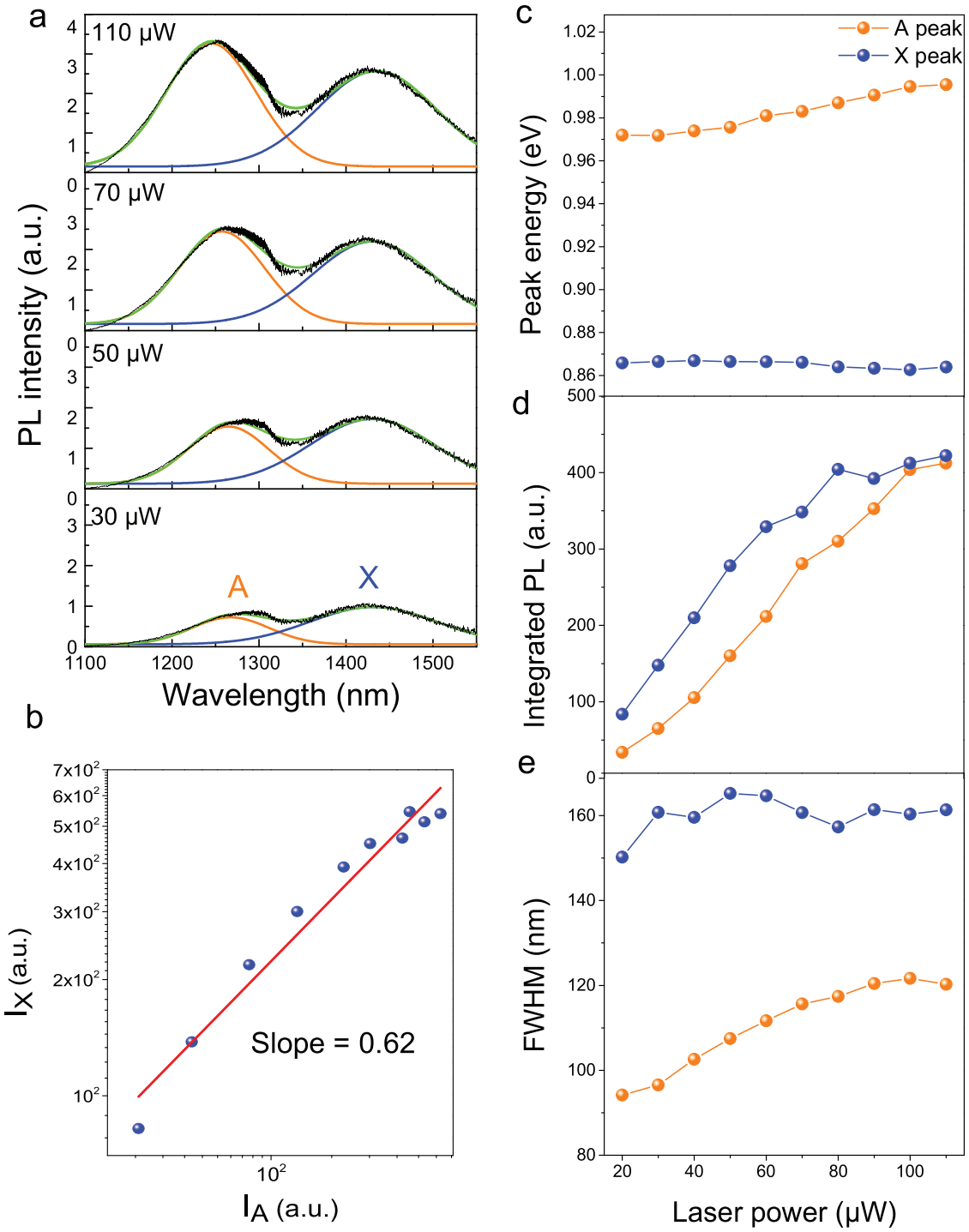

Figure 2. Power-dependent PL measurements. a) Measured PL spectra from 3L phosphorene samples over PECVD grown oxide layer at various excitation powers of the 532 nm laser. Spectrum have been fitted using 2 Lorentz peaks at ≈1250 nm (orange) and ≈1430 nm (blue). Green line shows the cumulative fit. b) Log–log plot showing the variation of integrated PL intensity of peak X as a function of peak A. From the fitting curve (red solid line) the PL intensity of peak X grows sublinearly ($\alpha \approx 0.62$), with the increase of the excitation power. c) Variation of A and X peak positions with the increase in laser power. d) Integrated PL intensity values plotted against laser power. e) Full width at half maximum (FWHM) variation with laser power. X peak's FWHM is independent of the laser power. A peak's FWHM (free excitons) shows an increase with increasing laser power due to enhanced thermal and phonon scattering at higher laser power.

oxide substrate with X peak appearing in all of them regardless of the material on which PECVD oxide substrate was sitting on (gold, silicon, and transparent quartz). We attribute the X peak to be from the localized excitons induced by the surface trapping centers from the PECVD substrate. Based on our Fourier-transform infrared (FTIR) spectroscopy measurements on

both PECVD and thermal oxides,[30] there are many dangling oxygen bonds on the PECVD oxide surface. The adatoms of O being absorbed on the surface of phosphorene can serve as exciton trapping centers, leading to the origin of sublevels and gap states in the bandgap of 3L phosphorene and giving rise to intermittent PL emission at lower energy levels.[44]

To study the thermal stability and activation energy of these localized states, we also performed the temperature-dependent PL measurements on the sample under the same excitation conditions. With the decreasing temperature, peak A was compromised for the enhancement of the X peak (**Figure 3**a). This trend can be explained with the schematic diagram shown in the Figure 3b. At low temperature, the localized and free excitons exist in their respective energy levels as shown. The thermal energy at low temperature is not enough to avoid the trapping of the free mobile excitons in defect sites and hence they can be localized/trapped and recombine radiatively to emit photons at 1430 nm.[45] At elevated temperatures (≈263 K), the thermal energy starts to increase which provides sufficient kinetic energy to the localized excitons to avoid trapping.[45] As shown in the Figure 3c, the peak positions are independent to the change of temperature. Whereas, the PL intensity of the X peak decays exponentially with the increasing temperature (Figure 3d). This trend can be explained by a theoretical model, which we used to fit the data for X peak in Figure 3d (solid red line). The localized excitons show a constant decay through a thermally activated dissociation channel, corresponding to the following decay equation[40]

$$\gamma = 1/[A\exp\{-E_a/k_BT\}] \quad (1)$$

where, γ is the PL intensity value observed, E_a is the activation energy of the localized excitons, k_B is the Boltzmann constant, A is an arbitrary fitting constant and T is temperature. The localized-state related PL emission shows characteristic thermal behavior, as shown in Figure 3. At low temperature, the generated excitons can get trapped by surface defects and impurities, due to relatively low kinetic energy of the excitons. Whereas, at high temperature the trapping efficiency decreases because of thermal activation of free excitons. Kato and Kaneko[46] and Xu et al.[45] suggested this relation between trapping efficiency and temperature. Therefore, it is expected that the intensity of localized exciton emission decreases monotonically with increasing temperature, which is exactly what we observed for the ones labeled as peak "X." The PL intensity of the "X" peak decreases with increasing temperature, which is because the excitons are not tightly bound to defects, and such weak interaction (shallow defect states) can be easily perturbed by thermal stimulation. E_a describes the necessary energy of thermal perturbation that prevents the free excitons from being trapped by localized defect sites.

The fitting equation gives the value of E_a ≈77.2 ± 0.1 meV. The extracted value for activation energy is smaller than the trapping potential demonstrated by the energy difference between the "A" and "X" peaks (≈130 meV). Similar observations have been made in other TMD and semiconducting materials as well (see Note S1 and associated Table S1, Supporting Information). The obtained activation energy of localized states in phosphorene is higher than what has been reported in localized emissions from 2D TMD materials such as WSe_2 (43 meV),[47] WS_2 (44.3 meV),[48] and other semiconducting materials such as InAs quantum dots (27 meV),[45] GaAs–AlGaAs nanowires (15 meV),[49] and GaN (27 meV).[50] Compared to a 2D system, the free excitons in phosphorene are confined in a quasi-1D space,[25,26] thus resulting in enhanced interactions with the defect sites.[51] The increased interaction requires higher activation energy correspondingly to overcome the trapping into defect states, because of which there is a greater stability of these localized exciton emissions even at temperatures close to room temperature ($E_a > k_BT$). High activation energy for the defect was simulated for phosphorene[52] and demonstrated for 1D CNTs recently.[51] For the free exciton peak (A peak), FWHM decreases at lower temperature again due to decrease in thermal and phonon scattering as explained earlier. Whereas, the FWHM of the X peak is again independent of the temperature, further suggesting its different nature with free excitons (Figure 3e). The total linewidth obtained can be theoretically explained by the following equation[53] which taken in to account the temperature independent intrinsic term and temperature electron–phonon and surface defect scattering

$$\acute{\Gamma}(T) = \acute{\Gamma}_{0+}\sigma T + \acute{\Gamma}_{LO}\left(\exp\left(E_{LO}/K_bT\right) - 1\right)^{-1} \quad (2)$$

Here, $\acute{\Gamma}_0$ is the dominantly electron–electron scattering representing term, which is independent of the temperature. Whereas σ is the electron-acoustic/thermal phonon coupling coefficient. LO is the longitudinal optical phonon term. $\acute{\Gamma}_{LO}$ represents the strength of exciton–LO phonon coupling, E_{LO} is the LO phonon energy.[53,54] In case of the free excitons due to higher degree of freedom the electron–phonon coupling plays a dominant role, which is temperature dependent as shown in the second and third terms of the equation. Hence, the linewidth will increase as the temperature increases. While, in the case of localized excitons trapped in defect states the movement is further confined to a quasi 0D state, thus limiting their degree of freedom. This results in weaker phonon coupling and hence the electron–electron scattering dominates which is independent of the temperature. Hence for localized excitons the FWHM does not change with increasing temperature. This effect has been explained in detail in defect states in quantum carbon dots,[53] CdSe nanodots,[55] Au nanoclusters.[56]

To further explore the nature of the localized excitons, we performed incident polarization dependent PL measurements on these peaks by changing the incident angle ΘInterestingly, both the A and X peaks exhibited anisotropic behavior and showed the same polarization direction along the armchair direction of the phosphorene crystal (Figure S2a,b, Supporting Information).[8,14,30,34,35] This further suggests that the localized states are caused by point-defects, like O adatoms[57] absorbed on the phosphorene PECVD interface, since point-defects would not change the polarization of the exciton emissions.[58,59]

In order to determine the overall quantum efficiency of the X peak in comparison to the A peak, we measured the PL spectra at several different spots, where there were different amounts of trapping centers caused by the nonuniformity of PECVD deposition. Large changes were observed in the PL spectra obtained from various locations. **Figure 4**a,b shows the variation in PL

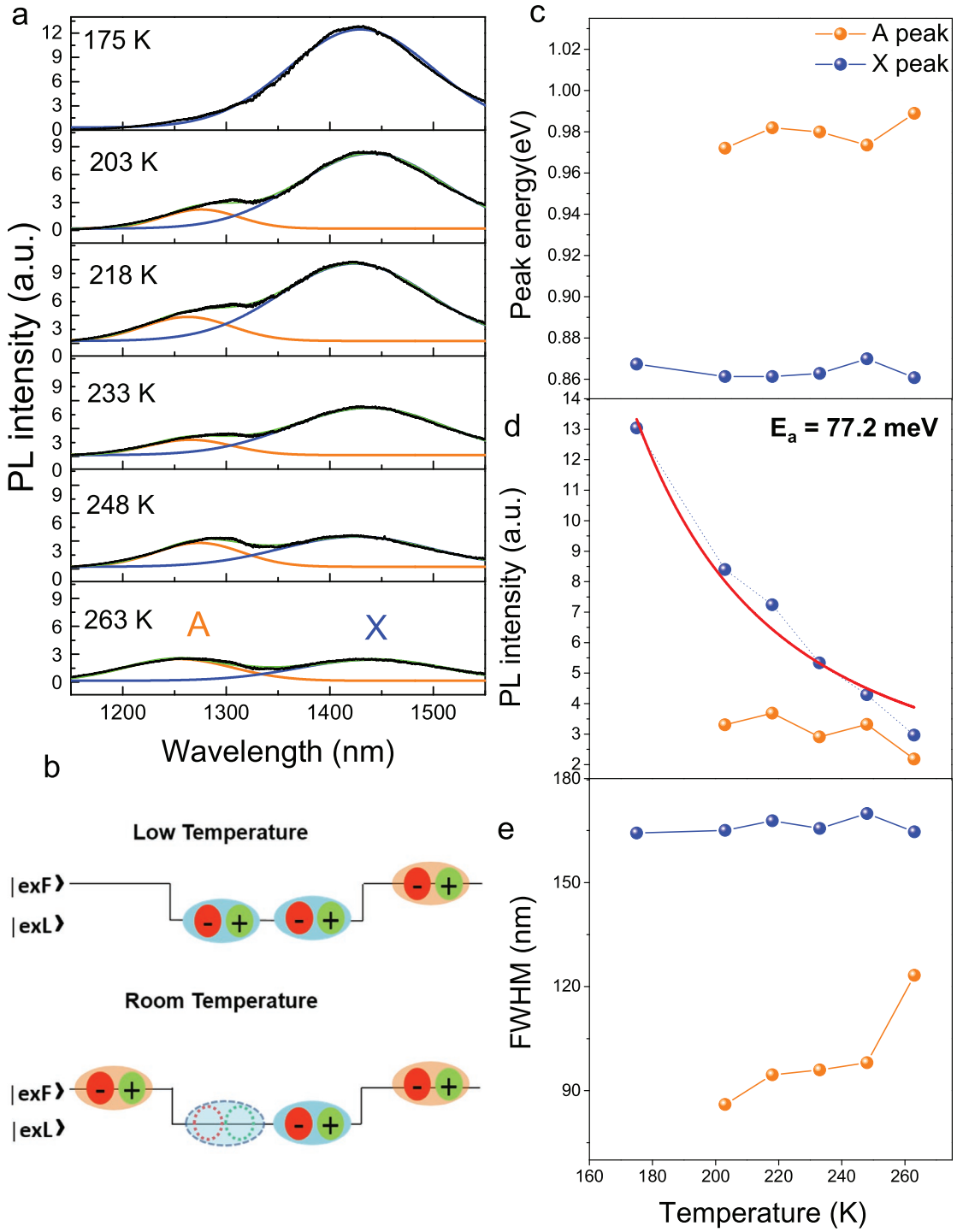

Figure 3. Temperature-dependent PL measurements. a) Measured PL spectra at various temperatures for phosphorene sample. b) Schematic diagram showing the position of localized (low energy) and free (high energy) excitons at low temperature and elevated temperatures. At higher temperature, the localized excitons gain sufficient thermal activation energy to move up to the free exciton energy level. c–e) Measured c) peak position, d) peak intensity and e) FWHM of PL peaks A and X as a function of temperature in 3L phosphorene. The PL intensity of peak X in (e) has been fit (red solid line) using the thermal exponential exciton decay equation (see main text) to calculate the thermal activation energy for localized excitons to be ≈77.2 meV.

spectrum obtained from two different positions. As the integrated PL intensity of peak A decreased, the integrated PL intensity for X peak increased considerably (Figure 4c). To determine the quantum efficiency of peak X as compared to the quantum emission efficiency of peak A, we followed the approach suggested by Miyauchi et al.[60] This approach is applicable to 1D matrix systems, and as shown above the free excitons in anisotropic phosphorene are confined to a quasi-1D space in nature

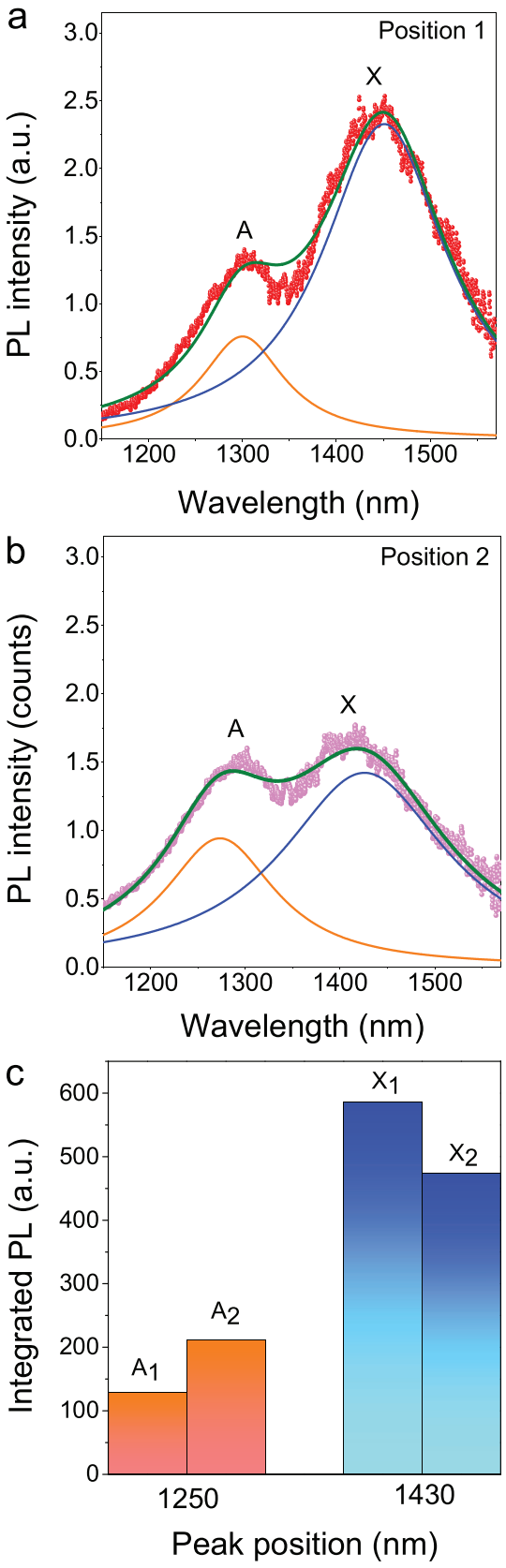

Figure 4. Internal quantum efficiency characterization. a,b) PL spectrum obtained from two different positions on the 3L phosphorene flake (See Figure 1), showing a varied ratio of peak A/peak X PL intensity. The orange peak shows the fitted peak "A" and blue peak shows the fitted peak "X." The green curve shows the cumulative fit peak. c) Integrated PL comparisons from the peaks at 1250 nm (blue) and 1430 nm (orange) respectively. The intensity of peak "A" increases while the intensity of peak "X" decreases in position 2 as compared to position 1. The change in integrated PL value was used to calculate the overall quantum efficiency enhancement of peak "X" with respect to peak "A."

(see Figure S2, Supporting Information). Thus, we can apply the same approach to determine overall quantum efficiency ratio between free excitons and localized excitons in case of phosphorene. Here, ΔI_X was defined in terms of the difference of two integrated PL intensities $\Delta I_X = |I_{X1} - I_{X2}|$, where, I_{X1} and I_{X2} are the two integrated PL intensities for localized exciton states measured at two separate locations. ΔI_A is the counterpart for free excitons. Matsuda and co-workers.[60] suggested an equation relating the $\Delta I_X/\Delta I_A$ ratio the internal quantum efficiency yield of the free excitons (η_A) and localized excitons (η_X) emissions as follows

$$\frac{\Delta I_X}{\Delta I_A} \sim \frac{1}{2}\left(\frac{\eta_X}{\eta_A}\right)\left(\frac{E_X}{E_A}\right) \quad (3)$$

We determined the value of $\frac{\eta_X}{\eta_A}$ to be ≈3.0. This indicates that the internal quantum efficiency of the localized excitons is slightly higher than that of free excitons. The enhancement is not as high as compared with what we observed from 1L phosphorene samples ($\frac{\eta_X}{\eta_A}$ ≈33.6) in our previous report.[30] This indicates layer-dependent defect emissions from phosphorene samples.

In addition, we also deposited bilayer (2L) phosphorene samples on PECVD substrate and measured the PL emissions, but we did not observe any defect peaks from 2L phosphorene samples. This could be depending on the electronic structure of the phosphorene layer and the properties of the adatoms. Similarly, 4L phosphorene samples were also prepared and measured. The free exciton peak emission from 4L is ≈1450 nm[35] which is close to the cutoff range of our InGaAs detector (900–1550 nm). Hence, we were unable to record any possible lower energy defect PL emission peaks from 4L sample, which would lie in the range >1550 nm. (see Figure S3 and associated text, Supporting Information). This opens avenues for further studies to confirm the layer-dependent extrinsic defect nature in mono- and few-layer phosphorene samples.

3. Conclusions

We have demonstrated an infrared PL emission at ≈1430 nm from 3L phosphorene, in addition to a free exciton emission at ≈1250 nm, by engineering the phosphorene–substrate interfacial states. The localized exciton emission is attributed to the extrinsic defect states caused by the adsorption of O adatoms on the surface of phosphorene. We confirmed the nature of these localized excitonic emissions using power-dependent

and polarization-dependent PL measurements. Temperature-dependent PL measurements were used to determine the activation energy (≈77 meV) of the localized excitons. This relatively high activation energy leads to the thermal stability of localized states in phosphorene, allowing them to be observed at elevated temperatures, in sharp contrast with other TMD materials. Our results have promising potential applications in future optoelectronic devices, such as chip-based optical telecommunication and photodetection devices.

4. Experimental Section

Few-layer phosphorene samples (2L–4L) were mechanically exfoliated onto the PECVD oxide (223 nm) on gold substrate with the thickness of gold ≈300 nm. Other sample were grown on normal silicon substrate covered with 280 nm of thermally grown SiO_2 respectively. The Au layer was used to fully block the influence of PL emissions from Si substrate in the first case, in order to avoid any discrepancy coming from the intrinsic defects in silicon being used. Due to high reflective nature of gold, it prevents any emission coming from underneath the gold surface to affect the PL emission detected from the phosphorene sample deposited over the other side of gold surface. This was necessary to understand the exclusive effect PECVD oxide in introducing stimulated defect emissions from few-layered phosphorene. PECVD oxide was deposited at 200 °C with SiH_4 and N_2O as reacting precursors, using the Plasmalab 100 dual frequency system. 3L phosphorene samples were put into a temperature-controlled chamber. All PL spectra, power-dependent PL and polarization-dependent PL measurements were conducted at a temperature of 263 K in the same microscope compatible chamber (LINKAM THMS 600), using a 532 nm Nd:YAG laser as the excitation source. Our PL system (T64000) uses two liquid nitrogen cooled detectors, one charge-coupled device (CCD) detector and one InGaAs detector.

Supporting Information

Supporting Information is available from the Wiley Online Library or from the author.

Acknowledgements

A.S., B.W., and B.L. contributed equally to this work. The authors thank Professor Chennupati Jagadish and Professor Barry Luther-Davies from Australian National University, for their facility support. The authors acknowledge financial support from ANU PhD student scholarship, China Scholarship Council, Australian Research Council, and ANU Major Equipment Committee.

Conflict of Interest

The authors declare no conflict of interest.

Keywords

activation energy, defect emissions, infrared, localized excitons, phosphorene

Received: December 29, 2017
Revised: February 6, 2018
Published online:

[1] M. Buscema, D. J. Groenendijk, S. I. Blanter, G. A. Steele, H. S. J. van der Zant, A. Castellanos-Gomez, *Nano Lett.* **2014**, *14*, 3347.
[2] R. Fei, L. Yang, *Nano Lett.* **2014**, *14*, 2884.
[3] X. Hong, J. Kim, S.-F. Shi, Y. Zhang, C. Jin, Y. Sun, S. Tongay, J. Wu, Y. Zhang, F. Wang, *Nat. Nanotechnol.* **2014**, *9*, 682.
[4] L. Li, Y. Yu, G. J. Ye, Q. Ge, X. Ou, H. Wu, D. Feng, X. H. Chen, Y. Zhang, *Nat. Nanotechnol.* **2014**, *9*, 372.
[5] H. Liu, A. T. Neal, Z. Zhu, Z. Luo, X. Xu, D. Tománek, P. D. Ye, *ACS Nano* **2014**, *8*, 4033.
[6] F. Xia, H. Wang, Y. Jia, *Nat. Commun.* **2014**, *5*, 4458
[7] A. Chaves, T. Low, P. Avouris, D. Çakır, F. Peeters, *Phys. Rev. B* **2015**, *91*, 155311.
[8] R. Xu, J. Yang, Y. Zhu, H. Yan, J. Pei, Y. W. Myint, S. Zhang, Y. Lu, *Nanoscale* **2016**, *8*, 129.
[9] J. Pei, J. Yang, R. Xu, Y.-H. Zeng, Y. W. Myint, S. Zhang, J.-C. Zheng, Q. Qin, X. Wang, W. Jiang, Y. Lu, *Small* **2015**, *11*, 6384.
[10] J. Pei, J. Yang, X. Wang, F. Wang, S. Mokkapati, T. Lü, J.-C. Zheng, Q. Qin, D. Neshev, H. H. Tan, C. Jagadish, Y. Lu, *ACS Nano* **2017**, *11*, 7468.
[11] J. Lu, J. Yang, A. Carvalho, H. Liu, Y. Lu, C. H. Sow, *Acc. Chem. Res.* **2016**, *49*, 1806.
[12] J. Pei, J. Yang, Y. Lu, *IEEE J. Sel. Top. Quantum Electron.* **2017**, *23*, 206.
[13] V. Tran, R. Soklaski, Y. Liang, L. Yang, *Phys. Rev. B* **2014**, *89*, 235319.
[14] R. Xu, S. Zhang, F. Wang, J. Yang, Z. Wang, J. Pei, Y. W. Myint, B. Xing, Z. Yu, L. Fu, *ACS Nano* **2016**, *10*, 2046.
[15] B. Radisavljevic, A. Radenovic, J. Brivio, V. Giacometti, A. Kis, *Nat. Nanotechnol.* **2011**, *6*, 147.
[16] J. S. Ross, S. Wu, H. Yu, N. J. Ghimire, A. M. Jones, G. Aivazian, J. Yan, D. G. Mandrus, D. Xiao, W. Yao, X. Xu, *Nat. Commun.* **2013**, *4*, 1474.
[17] J. Yang, R. Xu, J. Pei, Y. W. Myint, F. Wang, Z. Wang, S. Zhang, Z. Yu, Y. Lu, *Light: Sci. Appl.* **2015**, *4*, e312.
[18] Z. Yi, Y. Jiong, Z. Shuang, M. Salman, P. Jiajie, W. Xinghua, L. Yuerui, *Nanotechnology* **2016**, *27*, 135706.
[19] H. Nan, Z. Wang, W. Wang, Z. Liang, Y. Lu, Q. Chen, D. He, P. Tan, F. Miao, X. Wang, *ACS Nano* **2014**, *8*, 5738.
[20] Z. Lin, B. R. Carvalho, E. Kahn, R. Lv, R. Rao, H. Terrones, M. A. Pimenta, M. Terrones, *2D Mater.* **2016**, *3*, 022002.
[21] H. Chen, J. Yang, E. Rusak, J. Straubel, R. Guo, Y. W. Myint, J. Pei, M. Decker, I. Staude, C. Rockstuhl, Y. Lu, Y. S. Kivshar, D. Neshev, *Sci. Rep.* **2016**, *6*, 22296.
[22] H. Chen, V. Corboliou, A. S. Solntsev, D.-Y. Choi, M. A. Vincenti, D. de Ceglia, C. de Angelis, Y. Lu, D. N. Neshev, *Light: Sci. Appl.* **2017**, *6*, e17060.
[23] X. Zai-Quan, Z. Yupeng, W. Ziyu, S. Yuting, H. Wenchao, X. Xue, Y. Wenzhi, X. Yunzhou, S. Litao, Z. Changxi, L. Yuerui, L. Lei, B. Qiaoliang, *2D Mater.* **2016**, *3*, 041001.
[24] I. Aharonovich, D. Englund, M. Toth, *Nat. Photonics* **2016**, *10*, 631.
[25] Y.-M. He, ClarkGenevieve, R. SchaibleyJohn, Y. He, C. ChenMing, J. WeiYu, DingXing, Q. Zhang, W. Yao, X. Xu, C.-Y. Lu, J.-W. Pan, *Nat. Nanotechnol.* **2015**, *10*, 497.
[26] S. Tongay, J. Zhou, C. Ataca, J. Liu, J. S. Kang, T. S. Matthews, L. You, J. Li, J. C. Grossman, J. Wu, *Nano Lett.* **2013**, *13*, 2831.
[27] S. Mouri, Y. Miyauchi, K. Matsuda, *Nano Lett.* **2013**, *13*, 5944.
[28] S. Tongay, J. Suh, C. Ataca, W. Fan, A. Luce, J. S. Kang, J. Liu, C. Ko, R. Raghunathanan, J. Zhou, F. Ogletree, J. Li, J. C. Grossman, J. Wu, *Sci. Rep.* **2013**, *3*, 2657.
[29] A. Martin, O. Alibart, M. De Micheli, D. Ostrowsky, S. Tanzilli, *New J. Phys.* **2012**, *14*, 025002.
[30] R. Xu, J. Yang, Y. W. Myint, J. Pei, H. Yan, F. Wang, Y. Lu, *Adv. Mater.* **2016**, *28*, 3493.
[31] J. Pei, X. Gai, J. Yang, X. Wang, Z. Yu, D.-Y. Choi, B. Luther-Davies, Y. Lu, *Nat. Commun.* **2016**, *7*, 10450.

[32] J. Qiao, X. Kong, Z.-X. Hu, F. Yang, W. Ji, *Nat. Commun.* **2014**, *5*, 4475.
[33] S. Zhang, R. Xu, F. Wang, J. Yang, Z. Wang, J. Pei, Y. W. Myint, B. Xing, Z. Yu, L. Fu, Q. Qin, Y. Lu, *arXiv:1411.6124*, **2014**.
[34] S. Zhang, J. Yang, R. Xu, F. Wang, W. Li, M. Ghufran, Y.-W. Zhang, Z. Yu, G. Zhang, Q. Qin, Y. Lu, *ACS Nano* **2014**, *8*, 9590.
[35] J. Yang, R. Xu, J. Pei, Y. W. Myint, F. Wang, Z. Wang, S. Zhang, Z. Yu, Y. Lu, *Light: Sci. Appl.* **2015**, *4*, e312.
[36] A. Favron, E. Gaufres, F. Fossard, A.-L. Phaneuf-Lheureux, N. Y. W. Tang, P. L. Levesque, A. Loiseau, R. Leonelli, S. Francoeur, R. Martel, *Nat. Mater.* **2015**, *14*, 826.
[37] Y. Yun, T. Yoshida, N. Shimazu, N. Nanba, Y. Inoue, N. Saito, O. Takai, *J. Surf. Finish. Soc. Jpn.* **2007**, *58*, 307.
[38] J. O. Island, G. A. Steele, H. S. van der Zant, A. Castellanos-Gomez, *2D Mater.* **2015**, *2*, 011002.
[39] J. Shang, X. Shen, C. Cong, N. Peimyoo, B. Cao, M. Eginligil, T. Yu, *ACS Nano* **2015**, *9*, 647.
[40] Y. You, X.-X. Zhang, T. C. Berkelbach, M. S. Hybertsen, D. R. Reichman, T. F. Heinz, *Nat. Phys.* **2015**, *11*, 477.
[41] P. Perlin, C. Kisielowski, V. Iota, B. Weinstein, L. Mattos, N. A. Shapiro, J. Kruger, E. R. Weber, J. Yang, *Appl. Phys. Lett.* **1998**, *73*, 2778.
[42] J. I. Pankove, *Optical Processes in Semiconductors*, Courier Corporation, New York, NY : Dover **1971**, p. 422.
[43] Y. I. Mazur, G. G. Tarasov, G. J. Salamo, in *Self-Assembled Quantum Dots, Lecture Notes in Nanoscale Science and Technology*, vol *1*, Springer, New York, NY **2008**, pp. 67–128.
[44] X. Yang, S. Guo, F. Chan, K. Wong, W. Ching, *Phys. Rev. A* **1991**, *43*, 1186.
[45] Z. Xu, Z. Lu, Z. Yuan, X. Yang, B. Zheng, J. Xu, W. Ge, Y. Wang, J. Wang, L. L. Chang, *Superlattices Microstruct.* **1998**, *23*, 381.
[46] T. Kato, T. Kaneko, *ACS Nano* **2014**, *8*, 12777.
[47] Z. Wu, Z. Luo, Y. Shen, W. Zhao, W. Wang, H. Nan, X. Guo, L. Sun, X. Wang, Y. You, *Nano Res.* **2016**, *9*, 3622.
[48] C. Backes, A. Mitioglu, V. Vega-Mayoral, D. Hanlon, J. Coleman, V. Ivanov, D. Maude, P. Plochocka, *Nanotechnology* **2016**, *27*, 425701.
[49] D. Rudolph, L. Schweickert, S. Morkötter, L. Hanschke, S. Hertenberger, M. Bichler, G. Koblmüller, G. Abstreiter, J. J. Finley, *New J. Phys.* **2013**, *15*, 113032.
[50] C. Wetzel, S. Fischer, J. Krüger, E. Haller, R. Molnar, T. Moustakas, E. Mokhov, P. Baranov, *Appl. Phys. Lett.* **1996**, *68*, 2556.
[51] Y. Miyauchi, M. Iwamura, S. Mouri, T. Kawazoe, M. Ohtsu, K. Matsuda, *Nat. Photonics* **2013**, *7*, 715.
[52] A. Ziletti, A. Carvalho, D. K. Campbell, D. F. Coker, A. C. Neto, *Phys. Rev. Lett.* **2015**, *114*, 046801.
[53] P. Yu, X. Wen, Y.-R. Toh, J. Tang, *J. Phys. Chem. C* **2012**, *116*, 25552.
[54] B. T. Diroll, C. B. Murray, *ACS Nano* **2014**, *8*, 6466.
[55] X. Wen, A. Sitt, P. Yu, Y.-R. Toh, J. Tang, *Phys. Chem. Chem. Phys.* **2012**, *14*, 3505.
[56] P. Yu, X. Wen, Y.-R. Toh, J. Tang, *J. Phys. Chem. C* **2012**, *116*, 6567.
[57] A. Carvalho, M. Wang, X. Zhu, A. S. Rodin, H. Su, A. H. C. Neto, *Nat. Rev. Mater.* **2016**, *1*, 16061.
[58] A. K. Arora, A. Ramdas, *Phys. Rev. B* **1987**, *35*, 4345.
[59] L. Eaves, D. Halliday, *J. Phys. C: Solid State Phys.* **1984**, *17*, L705.
[60] Y. Miyauchi, M. Iwamura, S. Mouri, T. Kawazoe, M. Ohtsu, K. Matsuda, *Nat. Photonics* **2013**, *7*, 715.